

# Monitoring Ion Therapy with a Compton Camera: Simulation Studies of the Clinical Feasibility

J.-L. Ley<sup>1</sup>, D. Dauvergne<sup>3</sup>, N. Freud<sup>2</sup>, J. Krimmer<sup>1</sup>,  
J. M. Létang<sup>2</sup>, V. Maxim<sup>2</sup>, M.-H. Richard<sup>1</sup>, and É. Testa<sup>1</sup>

<sup>1</sup>Univ Lyon, Université Claude Bernard Lyon 1, CNRS/IN2P3, Institut de Physique Nucléaire de Lyon, 69622 Villeurbanne, France

<sup>2</sup>Univ Lyon, INSA-Lyon, Université Claude Bernard Lyon 1, UJM-Saint Étienne, CNRS, Inserm, Centre Léon Bérard, CREATIS UMR 5220 U1206, F-69373, Lyon, France

<sup>3</sup>LPSC, Université Grenoble-Alpes, CNRS/IN2P3 UMR5821, F-38026 Grenoble, France

E-mail: jeanluc.ley@gmail.com

**Abstract.** The aim of irradiation monitoring during a treatment in ion therapy is to control in real time the agreement between the delivered dose and the planned treatment. In fact, the discrepancies might come from uncertainties such as the planning accuracy by itself, or by variations due to the positioning or the anatomical changes of the patient. This can lead to ion-range variations of a few millimeters. Several devices are under development over the world to detect secondary radiation, which are correlated to the dose deposited by incident ions [1]. Compton cameras are in particular investigated for their potential high efficiency to detect prompt-gammas [2-5]. The present work aims at discussing the clinical applicability of a Compton camera design by means of Monte Carlo simulations validated against measurements of single and coincidence rates.

This first part should be shorter (just speak about treatment uncertainties)

There is no validation of the simulation against experimental data. The abstract should provide a summary of the paper results

Submitted to: *Phys. Med. Biol.*

**Keywords:** Compton Camera, ion therapy, clinical applicability, Prompt gamma

**Contents**

<b>1</b>	<b>Introduction</b>	<b>3</b>
<b>2</b>	<b>Material and methods</b>	<b>4</b>
2.1	Simulation setup . . . . .	4
2.2	Hadronic models used in Geant4 . . . . .	6
2.3	Particles of interest . . . . .	6
2.4	Data treatment . . . . .	6
2.4.1	Ion beam time structure . . . . .	6
2.4.2	Coincidence . . . . .	8
2.4.3	Time of flight discrimination and energy cuts . . . . .	9
2.5	Reconstruction algorithm . . . . .	9
2.5.1	Line-cone algorithm . . . . .	9
2.5.2	LM-MLEM algorithm . . . . .	10
2.6	Precision estimation . . . . .	11
<b>3</b>	<b>Results</b>	<b>14</b>
3.1	CC efficiency . . . . .	14
3.2	Beam intensity . . . . .	14
3.3	Comparaison LM-MLEM vs Line cone reconstruction . . . . .	17
3.4	Compton camera precision . . . . .	17
<b>4</b>	<b>Discussion</b>	<b>19</b>

## 1. Introduction

The exploitation of the high ballistic precision of hadrontherapy is currently limited by treatment uncertainties such like patient mispositioning, organ motion or morphological changes between treatment fractions. These uncertainties lead to the definition of relatively large safety margins around the planning treatment volume. Moreover the optimal treatment fields with a better sparing of healthy tissues are often discarded to avoid the irradiation of tumor with an organ at risk located downstream. There is therefore a global consensus in the community that ion-range verification is one of the conditions required for a broader usage of hadrontherapy.

Several techniques have been considered worldwide for twenty years. Most of them rely on the detection of secondary radiations generated during nuclear reactions undergone by a fraction of incident ions. Among these secondary radiations, prompt gamma-rays (PG) has the advantage to be emitted almost instantaneously which could allow for online treatment verification. In addition to this temporal feature, most of PG have well-defined energies corresponding to discrete transitions of incident ions (for ions heavier than protons) or target nuclei (mainly carbon and oxygen). Three observables can be therefore considered: emission point, PG energy and time-of-flight (TOF). Various modalities have been investigated taking benefit from one or several observables: PG imaging with or without collimation (i.e. collimated gamma camera or Compton camera, respectively)

## 2. Material and methods

### 2.1. Simulation setup

The monitoring system consists of a beam hodoscope and Compton prototypes under development within a French collaboration (CLaRyS - Contrôle en Ligne avec Rayonnements Secondaires) including five institutions: IPN Lyon, CREATIS Lyon, LPC Clermont-Ferrand, CPP Marseille and LPSC Grenoble. The detectors detailed characteristics can be found in [?]. For the sake of simplicity, the beam hodoscope is not modeled in this study, which focuses on prompt gamma detection via the Compton camera prototype. A scheme of the simulation setup is given in Figure 1.

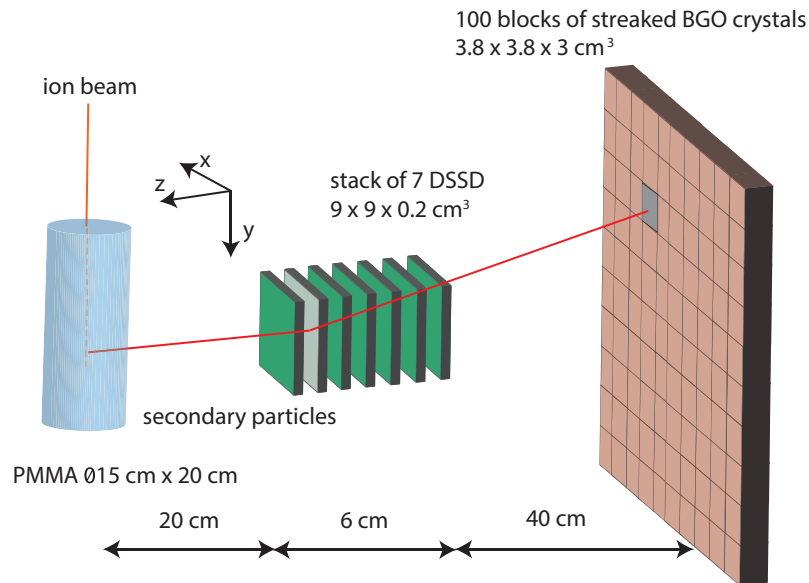


Figure 1: Model of the phantom (PMMA cylinder) and the Compton camera prototype. The Compton camera is composed of a stack of 7 DSSDs (scatterer) and a plan of 100 single BGO blocks. The set distances are realistic for clinical conditions. This configuration has been used for all the simulations presented in this paper.

Like most of the Compton camera devices, the CLaRyS prototype includes a scatterer and an absorber. The scatterer consists of seven parallel planes of silicon detectors (double-sided silicon strip detectors, DSSD),  $9 \times 9 \times 0.2 \text{ cm}^3$ , with 1 cm distance between the centers of two neighboring planes, while the absorber is composed of an array of  $10 \times 10$  BGO blocks ( $3.5 \times 3.5 \times 3.0 \text{ cm}^3$  each) placed at 40 cm from the last silicon layer (center-to-center distance). The ion beam interacts with a cylindrical PMMA† phantom (15 cm diameter and 20 cm length) placed in front of the Compton camera to mimic the patient body. It is placed 20 cm far from the first silicon plane (center-to-center distance) in order to fit with realistic clinical conditions. The silicon detectors have a strip pitch of 1.4 mm, for a total of 64 strips per side (double

sided readout based on electron and hole pairs collection). The strips are not reproduced in the simulation code, and the transverse spatial resolution is set to 0.9 mm FWHM at the reference energy of 1 MeV, according to preliminary measurements performed on small detector prototypes. Concerning the parallel direction, the interaction position is set to the center of the involved silicon plane.

Regarding the BGO blocks, their entrance surface is streaked in a  $8 \times 8$  matrix of pseudo-pixels,  $4.4 \text{ mm}^2$  side, and the readout is performed via 4 photo multiplier tubes. The position reconstruction is achieved via Anger logic for the real detector, but a mono-block crystal is simulated for simplicity. The events are selected to be limited to a single block component based on spatial analysis, and the interaction spatial resolution is set to 5 mm FWHM to fit with the geometrical features. For what concerns the parallel direction, given the fact that the employed BGO blocks have not depth of interaction reconstruction capabilities, the interaction position is fixed to the center of the mono-block crystal. (Put in the discussion some words about the possible improvement given by a new absorber with DOI capabilities)

Preliminary characterization measurements allowed to estimate the energy resolution of the BGO blocks, which is then set to 17% FWHM at the reference energy of 667 keV (a  $^{137}\text{cesium}$  source has been used for the measurements). The energy resolution of the silicon detector is set to 2.3 keV according to the design expectation; no characterization data are yet available for an instrumental estimate.

The time resolution has been set to 3.0 ns FWHM for the BGO blocks and to 15.0 ns FWHM for the silicon slabs, according to preliminary measurements performed on test detector modules at the GANIL (Grand Accélérateur National d'Ions Lourds) center in France.

(ALL THESE VALUES MUST BE VERIFIED -> see table 2) The detector resolutions play an important role in the Compton camera performances. The absorber spatial resolution influences the position of the apex of the Compton cone, as well as its axis orientation. The scatterer energy resolution determines the Compton cone aperture angle. The time resolution impacts the coincidence window between the absorber and the scatterer. As already mentioned, the hodoscope is not included in the simulation but its time resolution has to be taken into account for the time of flight discrimination. It is set to 1 ns FWHM.

The detector spatial, energy and time resolution are summarized in table 1.

Table 1: Estimations of reachable resolutions with the detectors. Those resolutions are applied during the simulations.

<b>Resolution (FWHM) at 1 MeV</b>	<b>Scatterer</b>	<b>Absorber</b>	<b>Hodoscope</b>
<b>spatial [mm]</b>	0.9	5	/
<b>energy [%]</b>	2.3	17	/
<b>timing [ns]</b>	15	3	1

## 2.2. Hadronic models used in Geant4

The Monte Carlo simulation study is performed with the Geant4 toolkit, version 9.6 patch 02. Geant4 has been developed by the CERN for high energy physics experiments, but it has been shown that it can be used for ion beam therapy studies [?, ?]. However, some improvements are still needed in order to extend the hadronic models to low energy applications[?].

The particle interactions in matter are described in this work by means of different models, listed in table 2. Additionally, the Doppler broadening and the photon polarization effects are taken into account.

Table 2: Hadronic models used in the Geant4 simulations.

Processus	Protons	Ions	Neutrons
<b>Electromagnetic</b>			
<b>Inelastic</b>	G4BinaryCascade	G4QMDReaction (G4IonsShenCrossSection)	standard <sub>option3</sub> G4BinaryCascade + G4NeutronHPInelastic (<19 MeV)
<b>Elastic</b>	G4LElastic	G4LElastic	G4LElastic + G4NeutronHPElastic (<19 MeV)
<b>Fission</b>	/	/	G4LFission + G4NeutronHPFission(<19 MeV)
<b>Capture</b>	/	/	G4LCapture + G4NeutronHPCapture (<19 MeV)
<b>Radioactivedecay</b>	/	G4Radioactivedecay	/

## 2.3. Particles of interest

The two main beam particles used in clinics are considered in this work: protons and carbon ions. The beam range of interest is 15.2 cm in the PMMA phantom, and the associated energy is 160 MeV for protons and 305 MeV/n for carbon ions.

In order to reproduce a realistic clinical beam, the beam transverse dimension is modeled with a gaussian distribution with a standard deviation of 5 mm for protons at 160 MeV and 3.5 mm for carbon ions at 305 MeV/n. The Compton camera setup does not change for the different incident particles. The beam intensity for a spot in pencil beam scanning (PBS) mode for protons is  $10^8$  particles and  $10^5$  particles for carbon ions. The beam time structure is applied in the data analysis stage, described below.

## 2.4. Data treatment

**2.4.1. Ion beam time structure** Two different beam time structures have been considered for this study, related to two kinds of accelerators used in clinical practice: the IBA C230 cyclotron for protons (used in 16 clinical centers worldwide) and the Heidelberg (Germany) synchrotron installed in the Ion Therapy Center (HIT) for carbon ions.

† PolyMethylMethAcrylate

† Bismuth Germanate

Even if the beam microstructure changes depending on the ion energy and the beam intensity, the microstructure at a specific energy and intensity is modeled in this work for simplicity. For protons at 160 MeV, the primary particles are grouped in bunches of 2 ns at a frequency of 106 MHz (9.42 ns) [?]. The clinical beam intensity is 3.2 nA which corresponds to about 200 protons per bunch. Concerning the carbon ion beam at 305 MeV/u, the estimated microstructure is composed of 30 ns bunches at a frequency of 5.9 MHz (170 ns). The clinical beam intensity for carbon ions is  $5 \times 10^7$  ions/s, corresponding to about 9 ions per bunch. This beam structure is extrapolated from measurements performed by our group in 2013 at HIT; the beam time structure was measured for 200 MeV/u and 400 MeV/u primary ion energy with a two scintillating fiber hodoscope (basic prototype of the one at present under development) and the spill signal was given by the accelerator. Figure 2 shows the beam structure for carbon ions at 400 MeV/u. The pulses have a spill period of 150.2 ns and each bunch is approximately 21.5 ns. The mentioned measurements have shown that the spill phase changes during the extraction: this implies that the HF signal from the synchrotron can not be used to locate the pulses, so that the use of the hodoscope seems required for time of flight background rejection purposes.

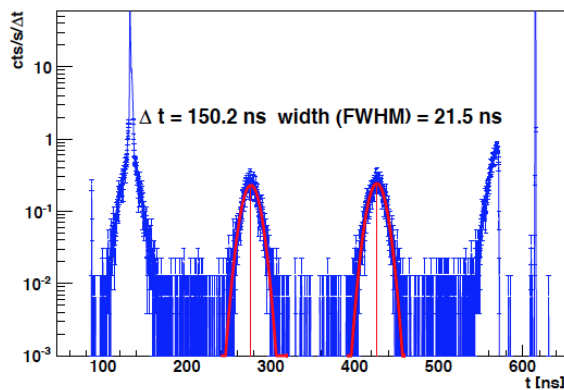


Figure 2: Time structure measured from a carbon ion beam at 400 MeV/u delivered at HIT. The pulses have an extraction period of 150.2 ns and the bunches are 21.5 ns FWHM. The measure was done with a two scintillating fiber hodoscope.

The coincidence window (between scatterer and absorber events) is set to 40 ns, centered on each absorber detected interaction. This value is adapted to the detectors time resolutions.

Table 3 resumes the presented beam time structures and coincidence reconstruction features.

Table 3: Description of the two beam structures studied: the IBA cyclotron C230 for protons and the synchrotron installed at the Heidelberg Ion Therapy Center (HIT) in Germany for carbon ions. The beam structures are applied to the simulation data.

		Protons	Carbon ions
Clinical features	<b>Facility</b>	IBA Cyclotron C230	Synchrotron at HIT
	<b>Clinical intensity</b>	$2 \times 10^{10}$ p/s	$5 \times 10^7$ ions/s
	<b>Energy</b>	160 MeV	305 MeV/u
Beam structure	<b>Bunch time [ns]</b>	3.2	30
	<b>Period [ns]</b>	9.4	170
	<b>Primaries /bunch</b>	217	9
Detectors	<b>Coincidence window [ns]</b>	40	40
	<b>Time resolution [ns]</b>	Si: 15 and BGO: 3	

**2.4.2. Coincidence** The Compton camera is based on a double interaction inside the scatterer and the absorber. A coincidence is defined as one energy deposit in the scatterer and one energy deposit in the absorber in a coincidence time windows given. A number of coincidence will be considered as background: quasi-simultaneous interaction from two secondary particles or a double interaction from the same particle different from a gamma.

If a coincidence is detected but the two particles are not coming from the same incident ion, the coincidence is named fortuitous. Otherwise, if a single particle from the same incident ion leaves energy in the absorber and the scatterer, the coincidence is named true.

It can be distinguish two types of true coincidence: a single gamma ray, which is a true gamma, and the rest of possibilities (electron, proton, neutron) which is background. The coincidences of interest are the true gamma.

The figure 3 resumes the different definitions of coincidences in the Compton camera.

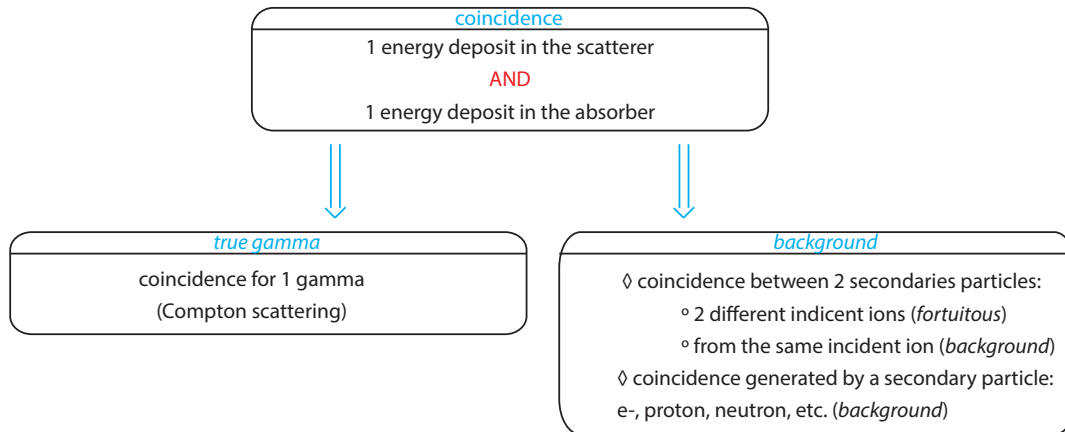


Figure 3: Diagram showing the different definitions of coincidences in the Compton camera.



### 2.4.3. Time of flight discrimination and energy cuts *Time of flight (TOF) information*

The goal is to eliminate the massive or charged particles (proton, electron, neutron) creating a coincidence in the Compton camera thanks to their speed. In fact, the photons are moving at the light speed when the other particles are moving slower due to their mass. To discriminate the particles with their speed, the time information coming from the hodoscope and the time information coming from the absorber are used. The difference between that information is named time of flight (equation 1). However, the hodoscope is not modelling in this study. As the Monte Carlo code consists to follow all stories individually, the time between the incident particle's creation and the secondary particle detection in the absorber is considered as the time of flight. Moreover, the hodoscope has a timing resolution about one nanosecond at full width at half maximum, so it is taking into account in the TOF estimation.

$$\begin{aligned} TOF_{theoretical} &= t_{absorber} - t_{hodoscope} \\ TOF_{simulation} &= t_{absorber} + t_{creation} + u_{hodoscope} \end{aligned}$$

With  $u_{hodoscope}$  the hodoscope resolution modelled by a Gaussian with a sigma of 1/2.35 ns.

The time of flight spectrum resulting from the simulation shows that the coincidences of interest are included in a window between 0 and 6 ns (figure 4). Therefore, all the coincidences with a TOF higher than 6 ns will be excluded from the results.

#### *Energy cuts*

Energy triggers are also defined for the detectors: 50 keV for the silicon layers and 100 keV for the absorber. An additional energy cut is practiced to the total energy absorbed in the camera and it is set at 1 MeV. In fact, the main gamma rays of interest have an energy upper at 1 MeV.

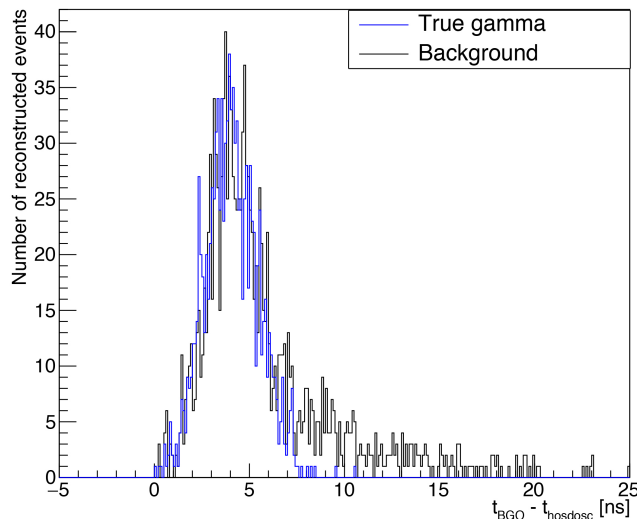
## 2.5. Reconstruction algorithm

**2.5.1. Line-cone algorithm** A simple method is used to reconstruct the emission position of the events detect in coincidence: the reconstruction line-cone. Thanks to the deposited energies in the detectors and the interaction positions, a cone is calculated which contains the event emission point. The energies enable to calculate the aperture of the Compton cone by way of the following equation:

$$\cos(\theta_{Compton}) = 1 - m_e c^2 \left( \frac{1}{E_{absorber}} - \frac{1}{E_{initial}} \right) \quad (1)$$

With  $E_{initial} = E_{absorber} + E_{silicon}$   
 $E_{absorber}$  the energy deposited in the absorber and  $E_{silicon}$  the energy deposited in the

Figure 4: Time of flight spectrum obtained by means of the simulation for a proton beam at 160 MeV and  $1 \times 10^8$  incident protons. The detection time for the absorber is given by the tag for the first deposit energy. The blue curve represents the time of flight for true events and the black one represents the background.



scatterer.

We assume that the initial energy of the gamma ray is fully absorbed in the absorber. This hypothesis combined to the detector energy resolutions lead to a potential uncertainty on the cone aperture. The interaction position in the scatter gives the cone apex and the position in the absorber gives the cone axis. The intersection of all the reconstructed cones gives the emission source point. In order to simplify the reconstruction and limit the possibilities, the beam direction is used to obtain just two solutions: the beam direction intersects the cone in two points. Only one of those solutions is the good one and the other will give a wrong information. As the original position is unknown when the gamma ray is detected in coincidence, the results presented in the next section take into account the two solutions.

*2.5.2. LM-MLEM algorithm* The iterative method allows to get a 3D image and allows to take into account the spatial resolution and the energy resolution of the detectors. Few iterative algorithms have been developed for the hadrontherapy [?, ?, ?, ?, ?].

The iterative algorithm *List-Mode Maximum Likelihood Expectation Maximization* (LM-MLEM) is a MLEM version which allows to free from sinograms and to reconstruct the image directly from the list of events detected.

The objective is to find the emission point of the gamma ray which produces the coincidence detected in the Compton Camera. The first step is to define the volume

which includes the origin of the prompt gamma ray detected. This volume is divided in equal voxels and the emission intensity is assumed homogeneous for each voxel  $j$  and follows a Poisson distribution of parameter  $\lambda_j$ . The vector contains the emissions intensities of all the voxels and the algorithm has to work it out. The system matrix  $T$  is composed of the coefficients  $t_{ij}$  which represents the probability that a photon produced by the voxel  $j$  is detected as a coincidence  $i$  by the Compton camera. The probability for a gamma detected in coincidence to be emitted by the voxel  $j$  is  $s_j$ . The LM-MLEM algorithm starts with an initial value  $\lambda^{(0)}$ , which can be the simple backprojection. The algorithm iterations are given by the following recurrence relation:

$$\lambda_j^{(l+1)} = \frac{\lambda_j^{(l)}}{s_j} \sum_{i=1}^{N_\gamma} t_{ij} \frac{1}{P_i^{(l)}}, \quad \text{avec} \quad P_i^{(l)} = \sum_{k=1}^{N_v} t_{ik} \lambda_k^{(l)}, \quad (2)$$

where  $N_\gamma$  is the number of detected events and  $N_v$  is the number of voxels in the image.

The LM-MLEM algorithm used for this study is the one developed by the laboratory CREATIS in Lyon [?, ?, ?, ?].

For each photon detected, the matrix  $T$  is calculated by taking into account the uncertainties on the angle between the source and the scatterer and the angle between the scatterer and the absorber. The matrix elements  $t_{ij}$  are calculated by:

$$t_{ij} = K(\beta_i, E_{tot}) \frac{|\cos(\theta_{\overrightarrow{V_2 V_1}})|}{V_2 V_1^2} \int_{M \in v_j} \frac{|\cos(\theta_{\overrightarrow{V_1 M}})|}{V_1 M^2} h_i(M) dv, \quad (3)$$

where  $\beta_i$  is the Compton scattering angle,  $V_1$  the interaction position in the scatterer,  $V_2$  the interaction position in the absorber,  $h_i$  the spatial kernel which models the uncertainties on the Compton angle for each voxel  $M$ ,  $K(\beta_i, E_{tot})$  the differential cross section and  $v$  the reconstructed volume.

In order to simplify and speed up the work out of the  $t_{ij}$  matrix, the voxels located far from the cone are set to 0. The distance between the cone and the voxel is calculated for the center of the voxel. The spatial resolutions are not considered for the algorithm. The images are finally created from the matrix  $T$  thanks to Matlab software.

## 2.6. Precision estimation

It is critical to know the Compton camera precision in clinical conditions in order to associate a decision threshold during the treatment. The precision is equivalent to a shift between the treatment planning (reference) and the reality. The study compares the relative position between a reference profile (reconstructed emission vertex profile at high statistics) and profiles at lower statistics. The analysis is done for a reference profile obtained from an analytic (line cone) and an iterative (LM-MLEM) algorithms. The high statistic profile obtained with the line cone method corresponds to  $2 \times 10^{10}$  incident protons (figure 5a) and the one with the LM-MLEM method corresponds to

$1 \times 10^{10}$  incident protons (figure 5b). The *SmoothKern* method, with the Nadaraya-Watson regression, is used to smooth the reference profiles in order to minimize relative statistic fluctuations.

The region of interest (ROI) is from  $y = 0$  mm to  $y = +100$  mm knowing that the Bragg peak is located around  $y = +50$  mm. The reference profiles are modelled in the ROI by a linear combination named Non-Uniform Rational Basis Splines (NURBS).

In theory, a new independent profile should be simulated at low statistics. However, to speed up the analysis, a random draw from Poisson's law is done from the NURBS profile (5c and 5d). The low statistics of interest are from  $10^8$  to  $5 \times 10^9$  incident protons. The smallest distance between the NURBS profil and a low statistic profile is estimated thanks to the method  $\chi^2$ . For the  $\chi^2$  estimation, the low statistic profile is defined around the fall-off from  $y = +30$  mm to  $y = +70$  mm. The minimization process moves the profile at low statistics on 60 mm from  $-30$  mm to  $+30$  mm around the initial position with a step of 0.1 mm. At each move, the  $\chi^2$  is calculated as :

$$\chi^2 = \sum_{i=1} (y_{sample,i} - y_{NURBS,i})^2, \quad (4)$$

where  $y_{sample}$  is the value of the number of coincidences for the low statistic profile,  $y_{NURBS}$  is the value of coincidences for the reference profile NURBS (scaled at the same low statistic) and  $i$  the step number.

The global minimum correspond to the smallest distance between the two profiles. The figures 5e and 5f show the distribution of  $\chi^2$  calculated for a low statistic profile at  $10^8$  incident protons.

A total of a thousand profiles at the low statistic are generated (named realizations) and the  $\chi^2$  minimization is done for all those. The standard deviation of the distribution resulting of the thousand results give the precision of the camera for a given number of incident protons. The figure 5g and 5h show the distributions at  $10^8$  incident protons for the line cone and LM-MLEM algorithms.

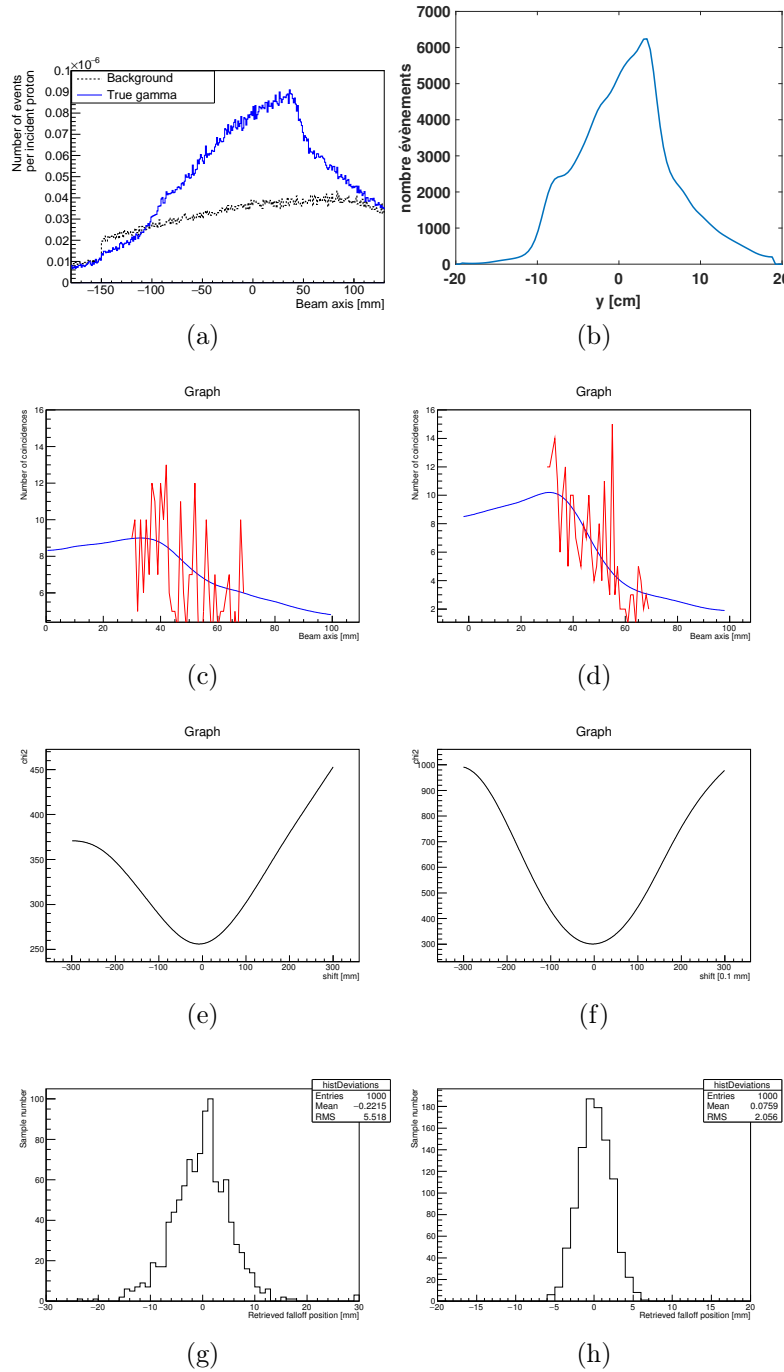


Figure 5: Treatment comparison for the same proton simulation with the line cone algorithm (left column: figures 5a, 5c, 5e, 5g) and the LM-MLEM algorithm (right column: figures 5b, 5d, 5f, 5h). The first row give the reconstructed profiles for  $2 \times 10^{10}$  incident protons (figure 5a) and for  $1 \times 10^{10}$  incident protons (figure 5b) respectively. The figures 5c and 5d are showing the reference curve (blue) and the estimated curve with Poisson's law at  $1 \times 10^8$  incident protons. The figures 5e and 5f are the  $\chi^2$  minimization results for one realization. The minimum of the curve gives the best fit between the reference curve and the low statistics one. Finally, the figures 5g and 5h represents the results for 1000  $\chi^2$  minimizations. The Compton camera precision is estimated thanks to the standard deviation of the distribution.

### 3. Results

#### 3.1. CC efficiency

The absolute efficiency is crucial for the Compton camera performances. It affects directly the number of detected events by the camera and so the reconstruction quality of those events. The absolute efficiency  $\epsilon$  is defined as :

$$\epsilon = \frac{N_{\gamma_{recons}}}{N_{\gamma_{total}}}, \quad (5)$$

with  $N_{\gamma_{recons}}$  the number of gamma events in coincidences,

$N_{\gamma_{total}}$  the total number of gamma emitted:  $10^8$ .

The absolute efficiency is presented in function of the localization of a monoenergetic gamma point source in comparison to the Compton camera center. The setup is the same as figure 1, but the point source is in the air and not in a PMMA phantom. The point source is moved from  $-300$  mm to  $+300$  mm with a step of  $20$  mm following the transverse axis of the camera (axis  $y$ ) and the gamma source is monoenergetic [300 keV, 6 MeV].

The figure ?? shows the absolute Compton camera efficiency in function of the gamma source position. The figure ?? gives the results without any cut in energy on the detectors and the figure ?? is with a cut applied on the energy deposited in the detectors: 50 keV for the scatterer and 100 keV for the absorber.

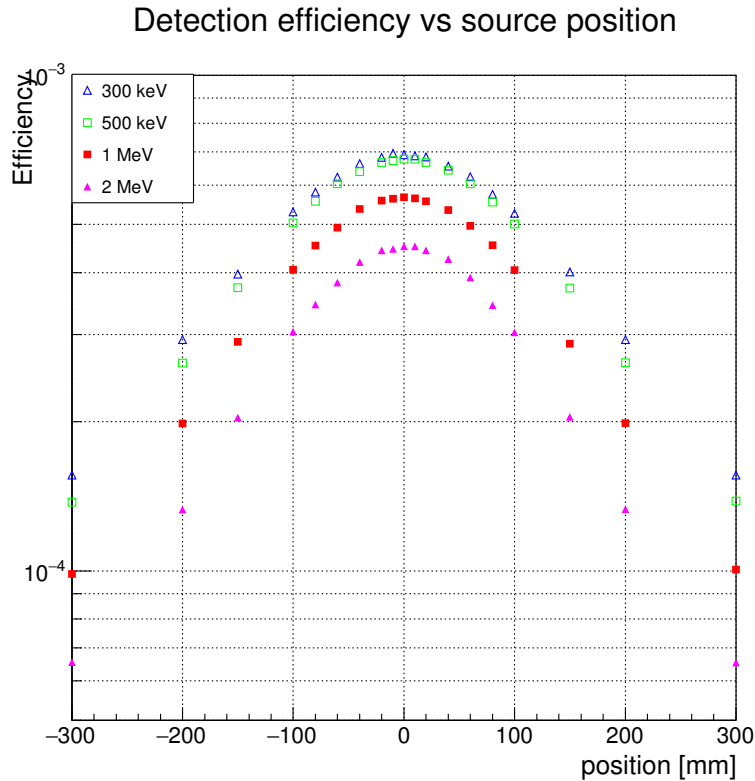
The absolute efficiency is between  $4 \times 10^{-4}$  at 300 keV and  $1.5 \times 10^{-4}$  at 6 MeV (figure ??). The efficiency is higher for low gamma energies because the probability of interaction in the absorber is decreasing with the energy. Moreover, when the point source is far from the camera center, the efficiency drops quickly. This effect is marked for high energies. In fact, the incident gamma will be less deflected in the scatterer for the same energy deposited compared to a low energy gamma. The incident gamma of interest in hadrontherapy are around 1 MeV, so it is important to well positioned the Compton camera to optimise the efficiency.

Another aspect to taking into account is the energy cut applied to the detectors (figure ??). The detectors are not perfect and cuts are mandatory to eliminate the electronic noise. If a gamma has a small Compton scattering angle, the energy deposited in the scatterer will be small. That is why, the camera efficiency decreases when the gamma source is centred with the camera. The limited energy cut is the one applied to the scatterer. This point is important to notice for an application of the Compton camera in nuclear medicine.

#### 3.2. Beam intensity

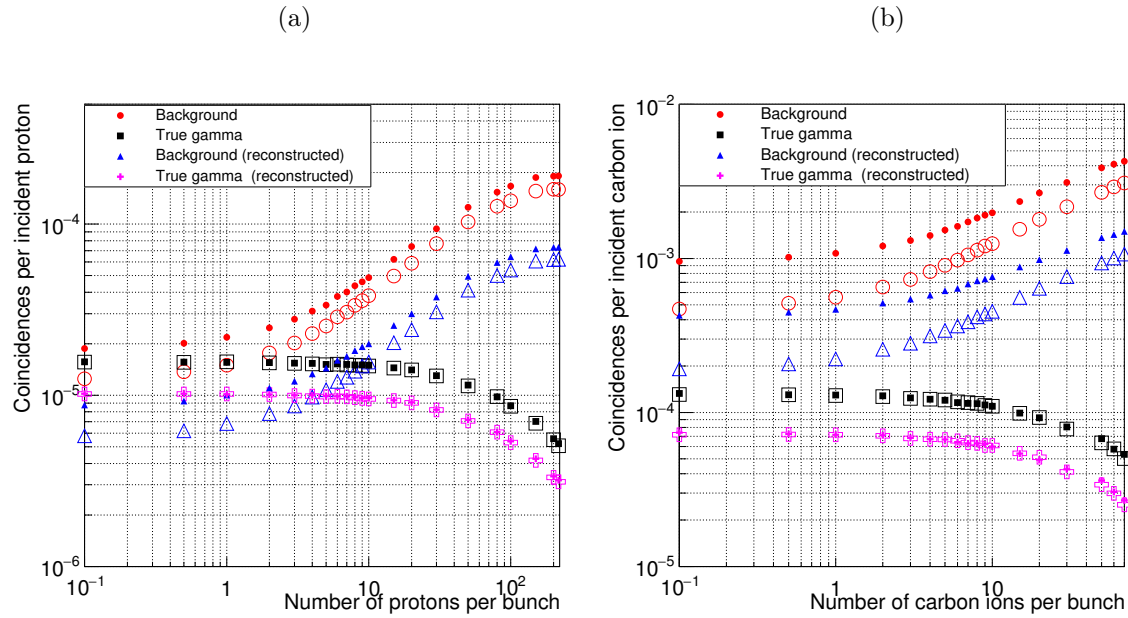
The beam intensity plays an important role for the Compton camera concerning its capability to distinct events in coincidence. In the simulation, the beam intensity is modeled by an average number of particles per bunch. The exact number of particles

Figure 6: Absolute Compton camera efficiency function of the gamma source position. The figure ?? shows the camera efficiency with no energy cut applied. It models the perfect Compton camera. The figure ?? takes into account cuts in energy: 50 keV for the scatterer and 100 keV for the absorber. The value of the energy cut can be different for the final prototype depending of the detector energy resolutions reach. The analysis is done for energies from 300 keV to 6 MeV.



in each bunch is given by a random draw in a Poisson distribution, where the mean value is the beam intensity chosen. The range of intensities was chosen in order to cover almost all the possibilities: from a very low beam intensity to the clinical beam intensity. Therefore, for proton and carbon ion, the lowest beam intensity is set to 0.1 particles per bunch in average and for protons goes up to 217 protons per bunch when in case of carbon ion, it goes up to 70 particles per bunch. The coincidence yields are scaled per ion incidents and the beam intensity per average ions per bunch. The true coincidences represent a coincidence in the camera by the same gamma ray. The background corresponds to all the other coincidence types. The simulations are done for a statistic of  $10^8$  in case of protons and  $2 \times 10^5$  for carbon ions. Those statistics correspond to the number of ions used in clinics to treat a spot.

Figure 7: Coincidences yield for protons (figure ??) and carbon ions (figure ??) in function of the beam intensity. The intensity is given for a number of incident particles per bunch. The distinction between the filled markers and the empty ones are the time of flight discrimination applied in the case of empty markers. Moreover, the yields are given before and after the profile reconstruction with the line cone algorithm.



At the clinical beam intensity, the high background level is mainly due to the random coincidences. In fact, the probability to detect two radiation coming from two different incident particles increases with the number of incident particles per bunch. Another issue is the single rate of events detected by each detector at those high intensities. For instance, at the clinic beam intensity in proton therapy, the single rate on the absorber is around 300 MHz and on the first silicon layer it is around 20 MHz. The current electronic front end and acquisition system are not able to treat this amount of data coming from all the detectors. As a result, it appears that it is impossible to use the Compton camera at a clinical beam intensity for the treatment monitoring in ion therapy.

Nevertheless, if the intensity decreases enough to avoid almost all the random coincidences, the monitoring seems more feasible. In addition, it can be supposed that the time of flight discrimination will improve the signal to the background ratio at low intensities by suppressing the coincidences induced by charged particles. Indeed, the charged particles are slower than gamma rays which move at the light speed.



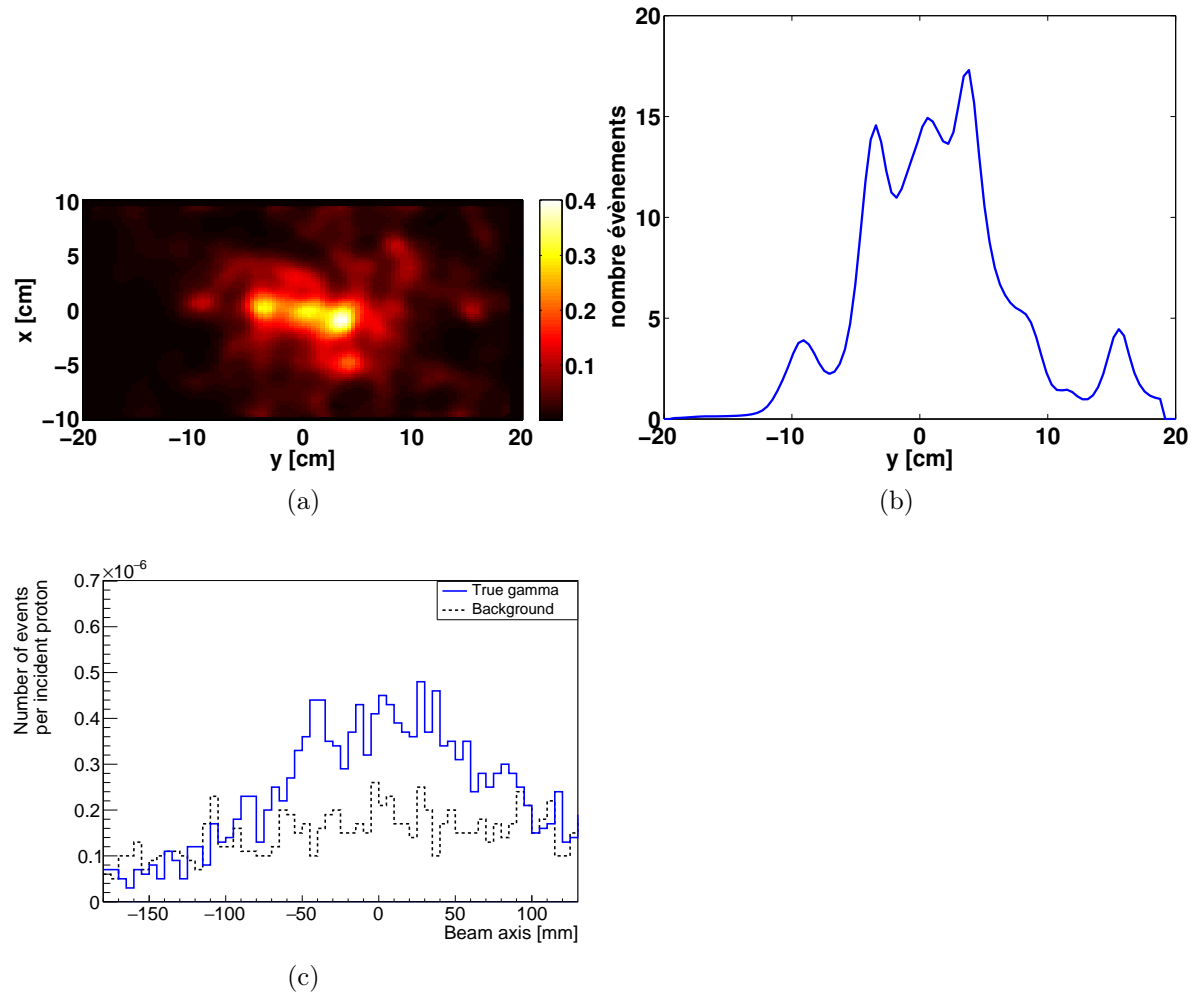


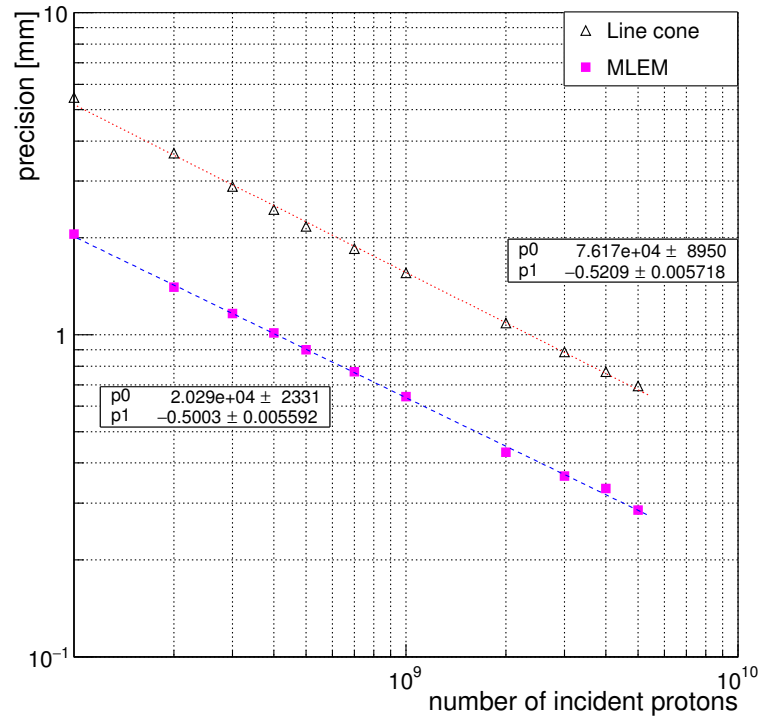
Figure 8: LM-MLEM reconstruction for a proton beam at 160 MeV and  $10^8$  incident protons. The events are detected in coincidence and the beam intensity is reduced to 1 proton per bunch. The PMMA target has a diameter of 15 cm and is 20 cm long. The Compton camera is centred at  $y = +50\text{mm}$ . The time of flight discrimination is applied and 20 iterations are realized. The figure ?? represents the reconstruction in 2D for the plan  $(x, y)$ . The position  $x = 0\text{mm}$  is the center of the PMMA phantom and  $y$  axis the direction of the proton beam. The figure ?? shows the profil corresponding to the figure ?? and following the axis  $y$ . The Bragg peak is localized at  $y = +50\text{mm}$ . The figure ?? is the profil obtained by means of line cone algorithm for the same simulation datas.

### 3.3. Comparaison LM-MLEM vs Line cone reconstruction

### 3.4. Compton camera precision

The information given by a control device as the Compton camera has to be viable and as precise as possible. In order to estimate the precision of the Compton camera, a method is used.

Figure 9: The Compton camera precision is estimated with two different algorithms: line cone and LM-MLEM. The precision is given for  $1 \times 10^8$  to  $5 \times 10^9$  incident protons. A linear fit is realized in order to obtain the slope of the results (p1 parameter). The graphic is scaled in log-log.



**4. Discussion**

bla bla

**References**